

Accepted Manuscript

Title: Electrochemistry and Chirality in Bibenzimidazole Systems

Author: Serena Arnaboldi Roberto Cirilli Alessandra Forni
Armando Gennaro Abdirisak A. Isse Voichita Mihali Patrizia
R. Mussini Marco Pierini Simona Rizzo Francesco Sannicolò



PII: S0013-4686(15)00796-3
DOI: <http://dx.doi.org/doi:10.1016/j.electacta.2015.03.177>
Reference: EA 24703

To appear in: *Electrochimica Acta*

Received date: 29-1-2015
Revised date: 21-3-2015
Accepted date: 24-3-2015

Please cite this article as: Serena Arnaboldi, Roberto Cirilli, Alessandra Forni, Armando Gennaro, Abdirisak A. Isse, Voichita Mihali, Patrizia R. Mussini, Marco Pierini, Simona Rizzo, Francesco Sannicolò, Electrochemistry and Chirality in Bibenzimidazole Systems, *Electrochimica Acta* <http://dx.doi.org/10.1016/j.electacta.2015.03.177>

This is a PDF file of an unedited manuscript that has been accepted for publication. As a service to our customers we are providing this early version of the manuscript. The manuscript will undergo copyediting, typesetting, and review of the resulting proof before it is published in its final form. Please note that during the production process errors may be discovered which could affect the content, and all legal disclaimers that apply to the journal pertain.

Electrochemistry and Chirality in Bibenzimidazole Systems

Serena Arnaboldi,^a Roberto Cirilli,^b Alessandra Forni,^c Armando Gennaro,^d Abdirisak A. Isse,^d
Voichita Mihali,^a Patrizia R. Mussini,^{a*} Marco Pierini,^e Simona Rizzo,^{c*} Francesco Sannicolò^a

^aUniversità degli Studi di Milano, Dipartimento di Chimica, Via Venezian 21, 20133 Milano, Italy

^bIstituto Superiore di Sanità, Dipartimento del Farmaco, Viale Regina Elena 299, 00161 Roma, Italy

^cIstituto di Scienze e Tecnologie Molecolari, C.N.R., Via Venezian 21, 20133 Milano, Italy,

^dUniversità degli Studi di Padova, Dipartimento di Scienze Chimiche, via Marzolo 1, 35131 Padova, Italy

^eUniversità di Roma “La Sapienza”, Dipartimento di Chimica e Tecnologie del Farmaco, Piazzale Aldo Moro 5, 00185 Roma, Italy

*Corresponding authors: Patrizia Romana Mussini, patrizia.mussini@unimi.it

Simona Rizzo, simona.rizzo@istm.cnr.it

Graphical abstract

Highlights

- More light on the electrochemical behaviour of imidazoles and biimidazoles.
- Relationship between conformational properties and electroactivity in biimidazoles.
- Different inherent chirality and electroactivity in 1,1'- and 2,2'-bibenzimidazoles.
- CV studies of 1,1'- bibenzimidazoles vs their single and double alkyl salts.
- A novel family of inherently chiral supporting electrolytes.

Abstract

A detailed electrochemical study has been carried out on 1,1'-bibenzo[*d*]imidazoles and the corresponding mono- and bibenzimidazolium salts, and compared to benzimidazole and benzimidazolium moiety models, and to 2,2'-bibenzo[*d*]imidazole constitutional isomers. The voltammetric experiments, supported by theoretical calculations and structural diffractometric characterizations, evidence how both electrochemical and chiral properties of bibenzimidazole systems depend on the torsional barrier between the two moieties, which determines at the same time the effective conjugation and communication between symmetrical redox centres, and the possibility of obtaining the molecule in two inherently chiral enantiomers that are configurationally stable at room temperature. In particular, the 1,1'-bibenzimidazole scaffold appears very promising for perspective development of inherently chiral substrates that may be used as additives, or supporting electrolytes, or ionic liquids. In fact, the high torsional angle granted by the 1,1' connectivity results both in an energy barrier high enough to yield permanently stable enantiomers at room temperature, and in low effective conjugation between the two moieties, affording a very large operating window. The effect of single and double alkylation has also been considered. A preliminary enantiorecognition test, achieved performing the electrooligomerization of enantiopure 2,2'-bi[2-(5,2'-bithienyl)]3,3'-bithianaphthene in the presence of either the (*R*)- or the (*S*)-enantiomer of a 1,1'-bibenzimidazolium salt, has shown interesting results.

Keywords: Inherently Chiral Electroactive Scaffolds; Inherently Chiral Supporting Electrolytes; bis-Benzimidazoles; bis-Benzimidazolium Alkyl Salts; Relationship between conformational properties and electroactivity

1. Introduction

Atropisomeric biheteroaromatic systems have been recognized as very versatile and accessible scaffolds to modulate both the steric and the electronic properties of suitable functional groups directly connected to them [1-6]. The electron density of such functional groups is influenced by the nature of the supporting heteroaromatic system, which can be more or less electron-rich, and also

by the position where they are located. Moreover, in biheteroaromatic systems, the nature of the heterocyclic rings influences the dihedral angle and consequently the steric characteristics of the molecule. In this context, a further advantage offered by biheteroarenes is the possibility of designing chiral functional materials endowed with outstanding chiroptical properties related to the presence of the inherently dissymmetric biaryl chromophore.

We have taken advantage of the biheteroaromatic strategy to prepare a successful modular series of chiral diphosphanes characterized by different phosphorous electronic availability and dihedral angle [6] and, very recently, electroactive oligothiophene macrocycles showing high chiroptical and enantiorecognition capacity [7-11].

The most satisfactory and promising functional materials we have prepared so far are based on electron-rich 3,3'-bithiophene [3,7-11] or 2,2'-bipyrrole scaffolds [2,4,12], whereas electron-poorer biheteroaromatic units have shown modest performances [4].

Recently, we have considered that 1,1'-bibenzimidazole, which is electron-poorer than 3,3'-bithianaphthene and, even more, than 2,2'- or 3,3'-biindoles [4], but easily accessible and easy to functionalize, could be employed as inherently chiral scaffold for the preparation of different materials, like non-conventional supporting electrolytes for chiral electrochemistry experiments and, if possible, inherently chiral ionic liquids, hopefully endowed with high chirality manifestations, like the above cited electron-rich inherently chiral materials.

The prerequisite for the correct development of the investigation was the electrochemical characterization of some model 2,2'-dialkyl-1,1'-bibenzo[*d*]imidazoles (**1a**, **1b** in Scheme 1) and the corresponding mono- and biimidazolium salts (**2a-b** and **3a-c** respectively). These experiments, supported by theoretical calculations and structural diffractometric characterization, are expected to shed light not only on the suitability of these compounds for applicative purposes but also on the electronic communication between the two heterocyclic moieties.

To have a comparison of the electronic effects involved when passing from a simple benzimidazole or its imidazolium salts to the corresponding biimidazole systems, the voltammetric investigation was extended to 1,2-dimethylbenzimidazole **4** and 1,2,3-trimethyl-benzimidazolium methanesulphonate **5**.

Furthermore, in order to gain information on the effects of electronic interaction between the benzimidazole rings in 2,2'-dialkyl-1,1'-bibenzo[*d*]imidazoles (**1**), we considered interesting to compare the voltammetric properties of these compounds, which are configurationally stable, with those shown by constitutional isomers 1,1'-dialkyl-1*H*,1'*H*-2,2'-bibenzo[*d*]imidazoles (**6a-b**), which are instead configurationally labile. In fact, compounds **6a-b** are devoid of a pair of substituents in position *ortho* to the interanular bond necessary to hinder rotation. Substrates **1b** and **6b** were selected for the comparative experimental evaluation, whereas scaffolds with methyl substituents **1a** and **6a** were chosen for comparison at computational level.

Finally, having succeeded in the resolution of (\pm)-**1a** by semi-preparative HPLC on a chiral stationary phase (CSP), we could prepare enantiopure bibenzimidazolium salts (*R*)- and (*S*)-**3a** and we could perform preliminary enantiorecognition tests, employing them as additives in the electrooligomerization of chiral 2,2'-bis[2-(5,2'-bithienyl)]3,3'-bithianaphthene (**BT₂-T₄**) monomer, both as enantiopure antipodes and as racemate [7-11] (Scheme 2).

2. Experimental

2.1. Synthesis

2.1.1. Synthesis of **1a** and **1b**

The 2-alkyl-1,1'-bibenzimidazoles **1a** and **1b** were prepared according to the general method previously reported by some of us [13].

2.1.2. Synthesis of 1,2,3 trimethyl-benzimidazolium methanesulfonate (**5**)

A mixture of 2-methylbenzimidazole (198 mg, 1.50 mmol), K₂CO₃ (310 mg, 2.24 mmol) and methyl methanesulfonate (0.2 mL) were heated at 80°C for 7 h. The crude reaction mixture was triturated with ethyl acetate and the undissolved solid was treated with methanol. The methanol solution was evaporated to dryness to give the title product as a brownish solid (m.p. > 300°C, 49% yield).

¹H NMR (300 MHz, DMSO): δ 8.05-8.02 (2H, m), 7.70-7.61 (2H, m), 4.01 (6H, s), 2.88 (3H, s), 2.31 (3H, s).

¹³C NMR (75 MHz, CD₃OD): δ 151.82 (s), 131.74 (s), 126.08 (s), 112.11 (s), 38.06 (s), 30.72 (s).

2.1.3. Synthesis of (±)-2,2'-dimethyl-3-methyl-[1,1'-bibenzo[d]imidazol]-3-ium methanesulfonate (**2a**)

A solution of 2,2'-dimethyl-1,1'-bibenzo[d]imidazole (**1a**) (50 mg, 0.19 mmol) and methyl methanesulfonate (0.018 mL, 0.21 mmol) in MeCN (0.2 mL) was heated at 80°C for 2.5 h. After removal of the solvent, the crude residue was repeatedly treated with diethyl ether to give the title product as a colourless solid (m.p. = 208-210°C, 97% yield).

¹H NMR (300 MHz, CDCl₃): δ 7.98 (1H, d, ³J (H,H) = 8.4 Hz), 7.89 (1H, d, ³J (H,H) = 7.8 Hz), 7.78 (1H, t, ³J(H,H) = 8.0 Hz), 7.63 (1H, t, ³J (H,H) = 8.0 Hz), 7.47 (1H, t, ³J (H,H) = 7.5 Hz), 7.37 (1H, t, ³J (H,H) = 7.5 Hz), 7.29 (1H, d, ³J (H,H) = 7.2 Hz), 7.14 (1H, d, ³J (H,H) = 8.4 Hz), 4.48 (3H, s), 3.02 (3H, s), 2.61 (3H, s), 2.59 (3H, s). ¹³C NMR (75 MHz, CDCl₃): δ 154.10 (s), 150.65 (s), 140.25 (s), 132.71 (s), 130.82 (s), 129.64 (s), 128.30 (s), 128.14 (s), 125.25 (s), 124.97 (s), 120.63 (s), 114.16 (s), 110.33 (s), 108.73 (s), 39.26 (s), 34.08 (s), 12.72 (s), 10.95 (s).

2.1.4. Synthesis of (\pm)-2,2'-dimethyl-3-hexyl-[1,1'-bibenzo[d]imidazol]-3-ium methanesulfonate (2b)

A solution of 2,2'-dimethyl-1,1'-bibenzo[d]imidazole (**1a**) (35 mg, 0.14 mmol) and hexyl methanesulfonate (0.02 mL, 0.14 mmol) in MeCN (0.2 mL) was heated at 80°C for 3.5 h. After evaporation of the solvent, the crude residue was repeatedly treated with diethyl ether to give the title product as an orange coloured oil (8% yield).

^1H NMR (300 MHz, CDCl_3): δ 7.96 (1H, d, $^3J(\text{H,H}) = 8.4$ Hz), 8.77 (1H, d, $^3J(\text{H,H}) = 8.1$ Hz), 7.75 (1H, t, $^3J(\text{H,H}) = 7.8$ Hz), 7.61 (1H, t, $^3J(\text{H,H}) = 7.8$ Hz), 7.45 (1H, t, $^3J(\text{H,H}) = 7.5$ Hz), 7.36 (1H, t, $^3J(\text{H,H}) = 7.5$ Hz), 7.24 (1H, t, $^3J(\text{H,H}) = 8.1$ Hz), 7.13 (1H, d, $^3J(\text{H,H}) = 8.1$ Hz), 5.00-4.34 (2H, m), 3.02 (3H, s), 2.60 (3H, s), 2.15-1.95 (2H, m), 1.59-1.28 (6H, m), 0.93 (3H, t, $^3J(\text{H,H}) = 6.9$ Hz). ^{13}C NMR (75 MHz, CDCl_3): δ 153.50 (s), 150.71 (s), 140.33 (s), 132.68 (s), 130.18 (s), 129.89 (s), 128.30 (s), 128.14 (s), 125.27 (s), 125.01 (s), 120.74 (s), 114.15 (s), 110.60 (s), 108.52 (s), 48.33 (s), 39.32 (s), 31.22 (s), 28.95 (s), 26.54 (s), 22.41 (s), 13.85 (s), 12.77 (s), 11.07 (s).

2.1.5. Synthesis of (\pm)-2,2',3,3'-tetramethyl-[1,1'-bibenzo[d]imidazole]-3,3'-diium methanesulfonate (3a)

A mixture of 2,2'-dimethyl-1,1'-bibenzo[d]imidazole (**1a**) (51 mg, 0.194 mmol) and methyl methanesulfonate (0.2 mL) was heated at 80°C for 3.5 h. The crude reaction mixture was repeatedly treated with diethyl ether and then with ethyl acetate to give the title product as a colourless solid (m.p. = 244 °C, 96% yield).

^1H NMR (300 MHz, CD_3OD): δ 8.27 (2H, d, $^3J(\text{H,H}) = 8.4$ Hz), 7.92 (2H, t, $^3J(\text{H,H}) = 7.5$ Hz), 7.86-7.73 (4H, m), 4.34 (6H, s), 2.98 (6H, s), 2.64 (6H, s). ^{13}C NMR (75 MHz, CD_3OD): δ 154.65 (s), 128.88 (s), 128.51 (s), 114.09 (s), 110.77 (s), 38.08 (s), 32.63 (s), 9.17 (s).

2.1.6. *Synthesis of enantiopure 2,2',3,3'-tetramethyl-[1,1'-bibenzo[d]imidazole]-3,3'-diium methanesulfonate ((-)-(R)-3a and (+)-(S)-3a)*

The experimental procedure was the same as described above for the synthesis of the racemate **3a**.

(-)-(R)-**3a**: m.p. = 241 °C, 96% yield; (+)-(S)-**3a**: m.p. = 241 °C, 92% yield).

2.1.7. *Synthesis of (±)-2,2'-dimethyl-3,3'-dihexyl-[1,1'-bibenzo[d]imidazole]-3,3'-diium methanesulfonate (3b)*

A mixture of 2,2'-dimethyl-1,1'-bibenzo[d]imidazole (**1a**) (470 mg, 1.79 mmol) and hexyl methanesulfonate (0.2 mL) was heated at 100°C for 71 h. The crude reaction mixture was repeatedly treated with diethyl ether to give the title product as a colourless solid (m.p. = 160-161°C, 18% yield).

¹H NMR (300 MHz, CDCl₃): δ 7.95 (2H, d, ³J (H,H) = 8.1 Hz), 7.88 (2H, d, ³J (H,H) = 8.1 Hz), 7.76 (2H, t, ³J(H,H) = 8.1 Hz), 7.68 (2H, t, ³J (H,H) = 8.1 Hz), 4.85-4.65 (4H, m), 3.12 (6H, s), 2.53 (6H, s), 2.30-2.12 (8H, m), 1.60-1.30 (8H, m), 0.95 (6H, t, ³J (H,H) = 6.9 Hz). ¹³C NMR (75 MHz, CDCl₃): δ 154.35 (s), 129.91 (s), 129.27 (s), 128.88 (s), 128.33 (s), 113.75 (s), 112.32 (s), 48.41 (s), 39.24 (s), 31.18 (s), 28.35 (s), 26.57 (s), 22.40 (s), 13.86 (s), 11.97 (s).

2.1.8. *Synthesis of (±)-3,3'-dimethyl-2,2'-dihexyl-[1,1'-bibenzo[d]imidazole]-3,3'-diium methanesulfonate (3c)*

A mixture of 2,2'-dihexyl-1,1'-bibenzo[d]imidazole (**1c**) (207 mg, 0.515 mmol) and methyl methanesulfonate (1.45 mL, 17.12 mmol) was heated at 40°C under stirring for 4 days. The crude reaction mixture was repeatedly treated with diisopropyl ether to give the title product as a brown hygroscopic oil. (147 mg, 46 % yield).

^1H -NMR (300 MHz, acetone- d_6): δ 8.31 (2H, d, $^3J(\text{H,H}) = 8.1$ Hz), 8.01 (2H, d, $^3J(\text{H,H}) = 8.7$ Hz), 7.88 (2H, t, $^3J(\text{H,H}) = 7.9$ Hz), 7.75 (2H, t, $^3J(\text{H,H}) = 7.9$ Hz), 4.49 (6H, s), 3.71-3.60 (2H, m), 2.49 (6H, s), 2.01-1.90 (1H, m), 1.80-1.65 (1H, m), 1.45-1.30 (2H, m), 1.25-1.10 (4H, m), 0.80-0.70 (3H, m). APT NMR 75 MHz, acetone- d_6): δ 157.52 (s), 131.64 (s), 130.16 (s), 128.41 (s), 128.16 (s), 114.56 (s), 111.45 (s), 38.68 (s), 33.65 (s), 30.93 (s), 28.61 (s), 26.29 (s), 26.21 (s), 21.98 (s), 13.24 (s). MS (ESI $^+$): m/z 431(16.7 %) (M^+ catione), 216 (100 %).

2.1.9. Synthesis of 1,1'-dihexyl-1H,1'H-2,2'-bibenzo[d]imidazole (**6**)

A heterogeneous mixture of 1H,1'H-2,2'-bibenzo[d]imidazole (234 mg, 1 mmol) anhydrous potassium carbonate (346 mg, 2.5 mmol) and dry acetonitrile (4 mL) was stirred at 25 °C for 10 min, then *n*-hexyl bromide (2.5 mmol, 0.35 mL) was added. The reaction mixture was heated for 24 h at 80°C. The mixture was filtered through a cell pad and, after evaporation of the solvent, the crude residue was purified by flash chromatography on SiO_2 (eluent mixture: hexane/ethyl acetate = 7/1). The title product was obtained as a yellow solid (m.p = 187-188 °C; 93% yield).

^1H -NMR (300 MHz, CDCl_3): δ 7.89 (2H, d, $^3J(\text{H,H}) = 6.0$ Hz), 7.52 (2H, d, $^3J(\text{H,H}) = 6.0$ Hz), 7.41-7.36 (4H, m), 4.91 (4H, t, $^3J(\text{H,H}) = 6.0$ Hz), 1.94-1.84 (4H, m), 1.84-1.29 (12H, m), 0.85 (6H, t, $^3J(\text{H,H}) = 6.0$ Hz). APT NMR (75 MHz, CDCl_3): δ 142.9 (s), 123.6 (s), 122.5 (s), 120.4 (s), 110.3 (s), 45.2(s), 31.2 (s), 29.9 (s), 26.4 (s), 22.4 (s), 13.9 (s).

Melting points were determined on a Büchi B-540 instrument. NMR spectra were recorded on Bruker AC 300 spectrometer (7 T). Chemical shifts are given in ppm and coupling constants in Hz. Mass spectra were recorded on VG 7070 EQ-HF instrument. Purifications by column chromatography were performed using silica gel Merck 60 (230 – 400 mesh for flash-chromatography and 70-230 mesh for gravimetric chromatography).

2.2. Polarimetry

Specific rotations were measured at five wavelengths (589, 578, 546, 436 and 365 nm) by a PerkinElmer polarimeter model 241 equipped with Na/Hg lamps. The volume of the cell was 1 mL and the optical path was 10 cm. The system was set at a temperature of 20 °C.

2.3. Circular dichroism

Circular dichroism spectra were measured by using a Jasco Model J-700 spectropolarimeter. The optical path and temperature were set at 0.1 mm and 25 °C, respectively.

The spectra are average computed over three instrumental scans and the intensities are presented in terms of ellipticity values (mdeg).

2.4. Crystallographic data for (±)-**1a**

Single crystal structural determination of (±)-**1a**. The intensity data for (±)-**1a** were collected on a Bruker Smart Apex CCD area detector using graphite-monochromated Mo K α radiation (λ = 0.071073 nm). Data reduction was made using SAINT programs; absorption corrections based on multiscan were obtained by SADABS [14]. The structures were solved by SHELXS-97 [15] and refined on F^2 by full-matrix least-squares using SHELXL-97 [15]. All the non-hydrogen atoms were refined anisotropically, whereas hydrogen atoms were included as ‘riding’ atoms and were not refined, except for one hydrogen atom bonded to a co-crystallized water molecule, whose coordinates have been refined imposing a DFIX restraint on the O–H distance. The other hydrogen atom of the water molecule was not located. The isotropic thermal parameters of H atoms were fixed at 1.2 (1.5 for methyl groups and the water molecule) times the equivalent thermal parameter of the atoms to which they are bonded. Crystal data and results of the refinement: colourless prism 0.45×0.42×0.15 mm, M_r = 1066.26, triclinic, space group P-1, a = 0.95812(10) nm, b = 1.13664(12)

nm, $c = 1.42600(15)$ nm, $\alpha = 108.478(2)^\circ$, $\beta = 98.953(2)^\circ$, $\gamma = 95.884(2)^\circ$, $V = 1.4357(3)$ nm³, $Z = 1$, $T = 296(2)$ K, $\mu = 0.078$ mm⁻¹. 19886 measured reflections, 5127 independent reflections, 4087 reflections with $I > 2\sigma(I)$, $3.82 < 2\theta < 50.26^\circ$, $R_{\text{int}} = 0.0256$. Refinement on 5127 reflections, 377 parameters, 1 restraint (DFIX). Final $R = 0.0410$, $wR = 0.1069$ for data with $F^2 > 2\sigma(F^2)$, $S = 1.036$, $(\Delta/\sigma)_{\text{max}} = 0.002$, $\Delta\rho_{\text{max}} = 0.188$, $\Delta\rho_{\text{min}} = -0.194$ e Å⁻³. CCDC 1046059 contains the supplementary crystallographic data for this paper. These data can be obtained free of charge from The Cambridge Crystallographic Data Centre via www.ccdc.cam.ac.uk/data_request/cif.

2.5. Computational methods

All calculations were performed by the computer program SPARTAN 08 (Wavefunction, Inc., Irvine, CA, USA). Ground states representative of the structure of 1,1'-dimethyl-1*H*,1'*H*-2,2'-bibenzo[*d*]imidazole and 2,2'-dimethyl-1,1'-bibenzo[*d*]imidazole were optimised by systematic algorithm based on molecular mechanic calculations (performed *in vacuo* with the MMFF force field), as implemented in SPARTAN 08. For 1,1'-dimethyl-1*H*,1'*H*-2,2'-bibenzo[*d*]imidazole just a minimum energy geometry was found, while two specular geometries (i.e. in enantiomeric relationship) were found for 2,2'-dimethyl-1,1'-bibenzo[*d*]imidazoles (i.e. the enantiomers (*S*)-**1a** and (*R*)-**1a**). The structure of one of these enantiomers and the ground state of 1,1'-dimethyl-1*H*,1'*H*-2,2'-bibenzo[*d*]imidazole were optimized at the B3LYP/6-31G(d) level of theory and afterwards submitted to single point energy calculation at a much higher level of theory, i.e. M062X/6-311+G(d,p) (a meta-hybrid GGA DFT functional).

Starting from the two possible geometries of **1a** having the aromatic rings in coplanar disposition (which were generated by hand), the same above described double step of DFT calculations were performed in order to obtain the relevant couple of transition state geometries TS1 and TS2 (Figure 3). These transition state geometries were also validated as saddle points by checking the presence among the evaluated vibrational modes of only one imaginary frequency, just corresponding to the rotation around to the N-N rings-junction.

The progressive change of energy as a function of the torsional angle N-C-C-N involving the C-C rings-junction

in 1,1'-dimethyl-1*H*,1'*H*-2,2'-bibenzo[*d*]imidazole was driven by the relevant algorithm implemented in SPARTAN 08, optimizing the single structures by the HF/3-21G method. Afterwards, the obtained geometries corresponding to the minimum (the ground state structure of 1,1'-dimethyl-1*H*,1'*H*-2,2'-bibenzo[*d*]imidazole) and maximum (the transition state structure of **6a**) of the assessed energy profile (see Figure 4) have also been submitted to optimization at the B3LYP/6-31G(d) level of theory and then to single point energy calculation at the higher M062X/6-311+G(d,p) level of theory. The correctness of the achieved geometry **6a**-TS as a saddle point through the B3LYP/6-31G(d) calculation was validated by checking the presence among the assessed vibrational modes of only one imaginary frequency, corresponding to the rotation around to the C-C rings-junction.

2.6. Electrochemistry

The model molecules were characterized by cyclic voltammetry, CV, in a wide scan range, using an Autolab PGSTAT potentiostat of Eco-Chemie (Utrecht, The Netherlands), run by a PC with the GPES software of the same manufacturer. The substrate working solutions (4 cm³) were 7.5×10^{-4} - 1.5×10^{-3} M in acetonitrile (Sigma-Aldrich, analytical grade on molecular sieves) with 0.1 M tetraethylammonium tetrafluoroborate (TEA)BF₄, (Aldrich, electrochemical grade) as supporting electrolyte; they were deaerated by N₂ purging before each experiment, the cell being equipped with a presaturator to grant constant working volume. The working electrodes were glassy carbon (GC) disks embedded in glass (0.031 cm², Metrohm). The optimised finishing procedure for the disk electrodes consisted in surface polishing with a diamond powder of 1 μm diameter (Aldrich) on a wet DP-Nap cloth (Struers). The counter electrode was a platinum disk. The reference electrode was an aqueous saturated calomel electrode (SCE) operating in a double bridge, filled with the working

medium, to avoid water and KCl leakage into the working solution. The ohmic potential drop was compensated by the positive feedback technique.

For the enantioselective electrooligomerization tests, conducting oligomer films were electrodeposited from racemic or enantiopure 5×10^{-4} M solutions of the 2,2'-bis[2-(5,2'-bithienyl)]3,3'-bithianaphthene (BT₂-T₄) monomer [7-11], both in the absence and in the presence of either the (*S*) or (*R*) enantiomer of **3a** in concentration of 10^{-3} M. The working medium and cell were the same as above. Electrooligomerization was achieved by performing 36 oxidative potential cycles at 0.2 V s^{-1} around the first oxidation peaks (*i.e.* between -0.39 and 0.96 V *vs.* Fc/Fc⁺), followed by repeated stability cycles in the same potential range in a monomer-free solution.

3. Results and Discussion

3.1. Synthesis of the substrates

Bibenzimidazoles **1a** and **1b** have been recently synthesized and characterized and their singular chromatographic behaviour interpreted on the basis of experimental HPLC on chiral stationary phase (CSP) [13].

We found that the preparation of bibenzimidazolium methanesulphonates **3** with long alkyl chains by direct alkylation of substrates **1** is not a simple reaction, since further alkylation of the mono-alkylated product requires rather drastic temperature conditions and long reaction times, which cause degradation with N-N bond cleavage. Furthermore, the purification of the imidazolium salts is not always an easy process. It is generally performed by repeated treatment of the alkylation mixture with suitable dry solvents such as diethyl ether, diisopropyl ether and ethyl acetate.

In addition, we succeeded in isolating both the enantiomers of the bibenzimidazolium salt **3a** in a pure state, starting from the enantiopure antipodes of **1a** obtained by semi-preparative HPLC resolution. The absolute configuration of the enantiomeric biimidazolium salts (–)-**3a** and (+)-**3a** is

that of the starting neutral antipodes, assigned by comparison of the CD curves of enantiopure (–)-**1a** and (+)-**1a** with those shown by (–)-**1b** and (+)-**1b**, for which the XRD structure was available (Figure 1) [13].

Compound **4** was already known in the literature and was prepared according to a reported procedure [16,17]. Alkylation with alkyl methanesulfonates is easy, even though purification of the products was unexpectedly difficult.

1,1'-Dihexyl-1*H*,1'*H*-2,2'-bibenzo[*d*]imidazole (**6b**) was obtained by double alkylation of bis-1*H*,1'*H*-2,2'-bibenzo[*d*]imidazole, prepared according to a known procedure [18], with *n*-hexyl-methanesulphonate in refluxing acetonitrile solution in the presence of potassium carbonate.

3.2. Single-crystal XRD characterization of (±)-**1a**

Crystals suitable for X-ray diffraction analysis have been obtained for (±)-**1a** by dissolving the compound in ethyl acetate and an ORTEP diagram is reported in Figure 2. The structure gives evidence of a π -stacked arrangement between benzimidazole moieties belonging to the (*R*) and (*S*) antipodes, and a nearly orthogonal arrangement of the two heterocyclic rings within each molecule, pointing to a hampered conjugative communication between them. The dihedral angles between the l.s. planes through the benzimidazole rings measure 81.27(4)° and 78.39(3)°, respectively.

3.3. Theoretical calculations

The geometries assumed by 2,2'-dimethyl-1,1'-bibenzo[*d*]imidazole (**1a**) and 1,1'-dimethyl-1*H*,1'*H*-2,2'-bibenzo[*d*]imidazole (**6a**), which are suitable models of compounds **1b** and **6b**, in their ground states have been modelled by DFT calculations (see section “*Computational methods*” for details).

According to its already described chiral nature [13], arising from the presence of a C_2 axis orthogonal to the N-N rings-junction as symmetry element, compound **1a** was found to exist as a couple of (*S*) and (*R*) enantiomers, with an angle of 90.5° formed by the aromatic planes junction

. Due to a high energy barrier that hinders their interconversion, the two (*S*) and (*R*) enantiomers manifest themselves as atropisomers. In fact, the racemate could be successfully resolved chromatographically on CSP [13]. By resorting again to DFT calculations (*i.e.* optimization of the relevant two possible transition states in which the bibenzimidazole rings are coplanar and the methyl groups are *syn*, TS1, or *anti*, TS2, with respect to the N-N junction), we have quantified such a barrier as 187.4 (TS1) and 192.9 (TS2) kJ mol⁻¹ (Figure 3).

On the contrary, just a single geometry has been assessed by DFT calculations for the 1,1'-dimethyl-1*H*,1'*H*-2,2'-bibenzo[*d*]imidazole (**6a**). In this structure, the aromatic bibenzimidazole planes are arranged in a perfectly coplanar conformation, featuring the methyl groups in *anti*-disposition (Figure 4). Instead, the alternative geometry, featuring the aromatic rings in coplanar conformation but with the methyl groups in *syn*-disposition (Figure 4), appears precluded as a possible ground state for the molecular system, because of the steric-hindrance arising from superimposition between the van der Waals spheres of the two very close alkyl substituents. Conversely, this structure has been assessed as a transition state **6a**-TS (*i.e.* the peak of the energy profile in Figure 4), which hinders the completely free rotation around the bond responsible for the C-C rings-junction, with an estimated energy barrier of 92.0 kJ mol⁻¹.

These results clearly afford a useful contribution to the rationalization of the electrochemical findings discussed below, suggesting the existence of a really effective π -conjugation between the bibenzimidazole frameworks in the case of the 1,1'-dimethyl-1*H*,1'*H*-2,2'-bibenzo[*d*]imidazole compound (**6a**), whereas a complete absence of π -conjugation is expected for **1a**.

The computational methods employed and the energies calculated for (*S*)-**1a** and **6a**, both at the ground state (GS) and transition state (TS), are reported in Table 1.

3.4. Voltammetric experiments

3.4.1. Neutral benzimidazoles

The relationship between structure and electronic properties in neutral 1,1-benzimidazoles can conveniently be investigated by cyclic voltammetry considering **1a**, taken as a model molecule, together with its corresponding half moiety **4**, plus molecules **6b** and **1b**, chosen to study the effects of bibenzimidazole connectivity (**6b**) and alkyl chain length at constant scaffold (**1b**).

Selected CV patterns in MeCN + 0.1 M (TEA)BF₄ are reported for the four molecules in Figure 5, whereas key CV parameters are reported in Table 2.

Notwithstanding its electron-poor nature, parent benzimidazole **4** features no reduction peak in the large potential window available, whereas an oxidation peak without a cathodic partner is observed at 1.13 V *vs* Fc/Fc⁺. The peak potential ($E_{p,a}$) of this peak varies linearly with $\log \nu$ with a slope ($\partial E_{p,a} / \partial \log \nu$) of 0.04 V, indicating a quasi-reversible electron transfer followed by a fast chemical reaction. According to the few literature studies [19,20] on systems of this kind, one-electron oxidation of 1-*H* imidazoles and benzimidazoles produces a radical-cation intermediate, which further reacts resulting in N,N electrooligomerization. Conversely, no film formation was observed with 1-methylimidazole consistent with the substitution on one of the nitrogen atoms. In accordance with the latter result, the CV pattern of **4** shows no evidence of electroactive film formation upon oxidation (Figure 5), although some electrode fouling was experimentally observed in oxidative voltammetry.

A reduction peak becomes neatly perceivable for the corresponding **1a** dimer, albeit very close to the background, at -3.02 V. Considering that the two moieties are nearly orthogonal, according to both XRD experiments and theoretical computations, the effect of increased conjugation should be very small. Thus, to justify the positive shift of the reduction peak potential, the electron withdrawing inductive effect of the benzimidazole group as substituent should be

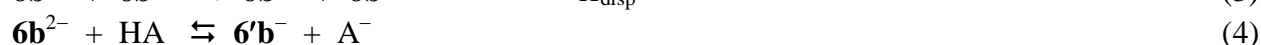
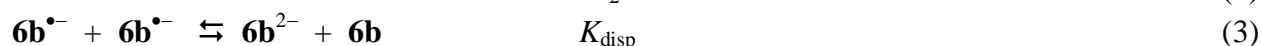
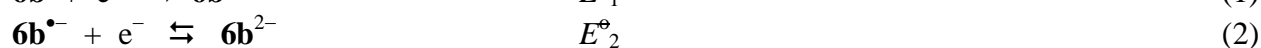
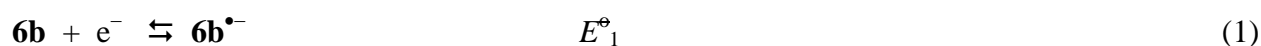
considered. This inductive effect would be consistent *inter alia* with the concurrent positive shift of the oxidation peak, which is very high (about 0.45 V). It might be justified considering that the same nitrogen atom, which in parent molecule **4** bears the electron donating methyl substituent, is in dimer **1a** directly attached to the electron-poor benzimidazole ring. Both the reduction and oxidation peaks of **1a** appear chemically and electrochemically irreversible; they should correspond to radical anion and radical cation formation and subsequent reactions, but a finer analysis is difficult since both processes are superimposed to the background onset. Rough estimates of $E_p - E_{p/2}$ and $\partial E_{p,a}/\partial \log v$ are reported in Table 2 only for the reduction peak, with values in line with a slow electron transfer. In any case, unlike the case of **4**, it is possible to precisely evaluate the potential window between first oxidation and first reduction peaks, which is very large, 4.6 V. This is a highly desirable feature of a material to be used as a chiral additive in electrochemical processes, as it is not reactive at the working potential, but may have some specific adsorption at the electrode surface favoured by the heteroatoms.

A comparison between the CV patterns of **1a** and **1b** allows one to evaluate the effect of the length of the aliphatic chain in 2 position. Such an effect appears to be nearly negligible, consistently with the similar inductive effects of the methyl and hexyl substituents [21], and with steric effects being in this case also very small.

Neat differences are instead observed by changing the connectivity from the 1,1' junction, present in **1a** and **1b**, to the 2,2' junction present in **6b**. Quite consistently with the calculated planar geometry in the closely related structure of **6a**, affording high effective π conjugation, both first oxidation and first reduction processes are shifted to more favourable potentials (both by about 0.4 V) with respect to **1a**, resulting in a much narrower potential window (by about 0.8 V).

Besides the narrower potential window, the CV pattern of **6b** shows significant differences with respect to that of **1a** or **1b**. Unlike these compounds, **6b** exhibits two cathodic peaks at -2.65 and -2.82 V and an anodic peak at -1.25 V. The first cathodic peak is partially reversible at low scan

rates, but becomes fully reversible at higher ν values. The effect of the scan rate on the voltammetric pattern of **6b** is illustrated in Figure 5e. As ν is increased, the normalized current density ($j/c\nu^{1/2}$) of the first peak decreases, while that of the second peak increases; the first cathodic peak tends also towards full reversibility and when at high scan rates this is attained, the two cathodic peaks become of the same height. Considering the presence of two equivalent and interacting units in the molecule, the two peaks may be attributed to two successive one-electron transfer processes yielding a radical anion and a dianion. The overall reduction process may be summarized by the following reaction sequence:



The first step is a reversible one-electron transfer yielding a radical anion intermediate with the negative charge probably centred mainly on one benzimidazole ring. Indeed, as expected for a reversible electron transfer, E_p does not significantly vary with the scan rate, whereas the half-peak width is $E_p - E_{p/2} = 0.057$ V. The second electron uptake, which is also reversible, occurs at more negative potentials because of the electronic communication between the two benzimidazole rings. The separation between the two reduction processes ($\Delta E^\circ = E_2^\circ - E_1^\circ$) depends on the degree of conjugation between the two equivalent units. The second electron transfer yields a dianion $\mathbf{6b}^{2-}$, a strong base, which is rapidly protonated to a monoanion $\mathbf{6'b}^-$ by any proton donor present in solution, probably the residual water. This peak does not show an anodic partner even at scan rates as high as 20 V s^{-1} . The anodic peak at -1.25 V may be attributed to the oxidation of the monoanion $\mathbf{6'b}^-$.

The intermediate radical anion can undergo a slow disproportionation reaction, which is avoided at relatively high scan rates. The equilibrium constant of disproportionation is related to the difference between the standard potentials of the two reduction steps.

$$K_{\text{disp}} = e^{F(E_2^\circ - E_1^\circ)/RT} \quad (5)$$

The standard potential of the first electron transfer can be calculated from cyclic voltammetry, when the reduction peak becomes reversible. However, E_2° is not accessible, which precludes precise determination of K_{disp} . If both electron transfers are reversible or quasi-reversible, which is the case of the present system, ΔE° may be approximately taken as the difference between the two peak potentials. Assuming $\Delta E^\circ = E_2^\circ - E_1^\circ \approx E_{\text{p,c}}^{\text{II}} - E_{\text{p,c}}^{\text{I}} = -0.170$ V, one obtains $K_{\text{disp}} \approx 1.3 \times 10^{-3}$.

As mentioned previously, the first oxidation peak of **6b**, is located at a significantly less positive potential than that of 1,1'-bibenzimidazole. By comparison with the first reduction peak it is surely monoelectronic. According to the voltammetric analysis ($\partial E_{\text{p,a}}/\partial \log v = 0.02$ V; $E_{\text{p,a}} - E_{\text{p,a}/2} = 0.041$ V), the process appears to be a fast electron transfer, followed by a fast, irreversible chemical reaction. This oxidation peak is followed by a complex multielectronic signal superimposed to the background current at 1.75 V, corresponding to the formation of an electrochemically active layer on the electrode.

On the basis of these results, the 1,1'-bibenzimidazole scaffold appears much more promising than its 2,2' analogue for perspective development of inherently chiral additives, or supporting electrolytes, or ionic liquids. In fact, only the high torsional angle granted by the 1,1' connectivity results both in an energy barrier high enough to yield permanently stable enantiomers at room temperature, and in low effective conjugation between the two moieties, affording a very large operating window.

3.4.2. Benzimidazolium salts

In the perspective of implementing the inherent chirality concept in charged species such as supporting electrolytes or ionic liquids, we have also investigated mono- and bis-alkylated 1,1'-

bibenzimidazoles, together with the parent benzimidazolium salt **5**, considering the six model compounds reported in Figure 6 and Table 3.

In all cases it is evident that alkylation makes the benzimidazole system much electron-poorer, resulting in easier reduction and more difficult oxidation. In fact, in contrast to the parent neutral compound **4**, which exhibited an oxidation peak in the available potential window, for the corresponding salt **5** a single reduction peak becomes visible at -2.51 V, whereas the oxidation peak is no more perceivable, being shifted beyond the background. The reduction process corresponds to a quasi-reversible electron transfer, followed by a fast, irreversible chemical reaction; no anodic partner was observed even at high scan rates.

Similarly, alkylation of bibenzimidazole **1** leads to a remarkable positive shift (1.2 - 1.4 V) of the first reduction peak, originally at *ca* -3.0 V. In particular, for the monomethyl salt **2a**, two reduction peaks are observed at -1.6 and -1.9 V at 0.2 V s⁻¹. Both peaks are irreversible and show no anodic partner up to the highest applied scan rate of 20 V s⁻¹. Both peaks shift cathodically with increasing v , with the first peak tending to merge into the second one at high scan rates. The values of the $\partial E_p/\partial \log v$ slope and half-peak width, reported in Table 3, indicate that both processes are under kinetic control of the electron transfer.

In the case of the monohexyl salt **2b**, a single reduction peak is observed at -1.9 V, *i.e.* the potential of the second reduction peak of **2a** (actually the CV patterns of **2a** and **2b** become increasingly similar with increasing scan rate). Also in this case, the reduction peak never shows an anodic partner and its peak potential varies linearly with $\log v$ with a slope of -0.033 V, indicative of a reversible electron transfer followed by an irreversible chemical reaction.

This intriguing difference between the voltammetric responses of **2a** and **2b** could be rationalized by assigning the first peak of **2a** to the uptake of one electron by the cation localized on the nitrogen site to give an alkyl radical species, which is further reduced to the corresponding carbanion at the second reduction peak (Scheme 3).

A similar reduction scheme may be proposed also for **2b**, but in this case the first electron uptake appears to be less favoured by changing the methyl substituent on the nitrogen cation of **2a** with a bulkier hexyl group (**2b**), resulting in a negative shift of the first reduction potential. In this light, the single reduction peak observed for **2b** could correspond to both radical formation and subsequent reduction to an anion, with a global uptake of two electrons. The reason for this significant dependence of the reduction potential of the cation on the nature of the alkyl group is not clear. It seems to be related more to the bulkiness of the group than to polar effects, which are quite similar for methyl and hexyl groups.

For both **2a** and **2b** a first oxidation signal can still be perceived, but at a more positive potential than **1a**, quite on the background, and resulting on the electrodeposition of an electrochemically active layer on the electrode surface (Figure 6).

A further positive shift, albeit much smaller, is observed for the first reduction peak of the double alkylated salts, consistent with the reciprocal inductive effect between the two alkylated moieties (**3a-c**). For the same reason, no neat oxidation peaks are perceivable in this case, albeit some enhancement of positive currents before the background discharge and some negative shift of the latter can be observed (hardly reproducible, depending on the electrode surface activation).

Unlike monoalkylated salts **2a** and **2b**, dialkylated dications **3a**, **3b** and **3c** (with alkyl chains of different lengths in either N or C positions) show essentially the same reduction CV patterns. In particular, an intense reduction peak, followed by a smaller peak is observed. The first peak is completely irreversible, whereas the second peak shows an anodic partner even at low scan rates. The voltammetric pattern is significantly modified when the scan rate is increased. The normalized current of the first peak considerably increases, while the second peak decreases and disappears at $v = 5 \text{ V s}^{-1}$. It appears that the overall reduction process at the first peak involves consumption of a fraction of the starting material, which does not undergo reduction. In other words, there is some type of a parent-child reaction, which subtracts part of the starting material from the reduction

process. The product of such a reaction is responsible for the second reduction peak. The parent-child reaction is avoided at relatively high scan rates, and consequently the charge consumption of the first peak increases because now the whole substrate undergoes reduction. Concurrently, the second peak disappears as the species responsible for this reduction process is no longer produced. The nature of these reactions was not further investigated.

By comparison with **2b**, reduction of dication **3a-3c** is expected to be a bielectronic process, and, considering the symmetry of the system and the lack of conjugation between the two moieties, it is likely to involve concurrent one-electron uptake by each imidazolium site.

3.4.3. Preliminary enantioselectivity test of (*R*)- and (*S*)-**3a** as additives in the electrooligomerization of **BT₂T₄** chiral monomer

To perform a preliminary enantioselectivity test of the new 1,1'-bibenzimidazolium salts, enantiopure (*R*)- and (*S*)-**3a** have been tested as stereoselection inductors for the electrooligomerization of the inherently chiral **BT₂T₄** monomer [7-11] (Scheme 2).

The electrodepositions were carried out using a 0.0005 M solution of either the (\pm)-**BT₂T₄** monomer racemate or the enantiopure (*R*)-**BT₂T₄** monomer, in MeCN + 0.1 TBAPF₆. In each case the experiment was performed (a) with **BT₂T₄** alone, (b) with addition of enantiopure (*R*)-**3a** in a 2:1 ratio, (c) in the presence of enantiopure (*S*)-**3a** in a 2:1 ratio. In all electrooligomerization tests, the oligomer films were deposited on GC electrode by performing 36 oxidative cycles around the first **BT₂T₄** oxidation peak, in a potential range where the chiral additives are not active. The 36th (*i.e.* last) oligomerization cycles are shown in Figure 7a (for racemate (\pm)-**BT₂T₄**, as such and with **3a** additives) and Figure 7c (for enantiopure (*R*)-**BT₂T₄** monomer, as such and with **3a** additives).

After the electrodeposition step the working electrode was extracted from the monomer solution and the stability of the oligomer film tested by performing oxidative cycles in the same

potential range, but in a monomer-free solution. The fifth stability cycles are shown in Figures 7b and 7d for racemate oligo-**BT₂T₄** and enantiopure oligo-(*R*)-**BT₂T₄** films, respectively.

Electrooligomerization regularly took place in all cases, but both the growth and the stability CV patterns were remarkably affected by the presence of the enantiopure additives. In the case of racemate (\pm)-**BT₂T₄** oligomerization, the presence of the additives resulted in a significantly slower electrodeposition. Notably, the same effect was observed working in the presence of either (*R*)-**3a** or (*S*)-**3a** (Figure 7a), which is consistent with electrooligomerizing the (\pm)-**BT₂T₄** racemate. The electrodeposited films also appear to be quite stable in subsequent stability cycles, in all cases (Figure 7b).

Performing the same electrooligomerization with enantiopure (*R*)-**BT₂T₄** in the absence of additives, the process is slower with respect to the racemate case (consistently with previous observations [7], and possibly as a consequence of the decrease in freedom degrees), and the CV pattern is more finely defined. However, both the oligomer oxidation onset and the maxima occur at potentials similar to those of the racemate, and again, the films are quite stable upon further cycling in monomer-free solution.

Instead, quite unlike the racemate case, the oligomerization CV patterns of (*R*)-**BT₂T₄** are significantly affected by the presence of either (*R*)-**3a** or (*S*)-**3a**; the CV patterns change in shape, onset and maxima potentials (Figure 7c), and also in stability in oxidative cycles in monomer-free solution (Figure 7d).

Such a significant difference can be justified assuming the existence of two diastereomeric situations, (*R*)-**BT₂T₄** in the presence of (*R*)-**3a** and (*R*)-**BT₂T₄** in the presence of (*S*)-**3a**, with neatly different energy and/or structural parameters. Thus, this test could provide a first evidence, albeit preliminary, of the enantioselection ability of the new family of inherently chiral compounds, even at low concentrations.

4. Conclusions

The 1,1'-bibenzimidazole scaffold is much more promising than its 2,2' analogue in the perspective of obtaining inherently chiral additives, or supporting electrolytes, or ionic liquids, capable of high enantioselectivity in chemical and electrochemical processes. In fact, only the high torsional angle granted by the 1,1' connectivity results in an energy barrier high enough to yield permanently stable enantiomers at room temperature, as well as in low effective conjugation between the two moieties, affording a very large operating window for neutral 1,1-benzimidazoles. For this reason these molecules appear promising chiral additives in stereospecific chemical and above all electrochemical processes, especially carried out on electrodes such as Au, Cu, Ag, etc., having specific affinity for amino compounds.

The corresponding alkyl salts, single or double, have a narrower potential window on the reduction side, but could also be applied as chiral supporting electrolytes, while for use as ionic liquids their melting points are still too high; this target might be achieved by succeeding in introducing four long alkyl chains instead of two and/or by changing the counteranions.

In any case, the enantiopure antipodes of a dialkylated salt gave quite promising results as additives in a preliminary chiral electrodeposition experiment, even though they were used at a very low concentration. This confirms the effectiveness of the "inherent chirality" concept in granting remarkable chirality manifestations, already evidenced in bibenzothiophene scaffolds and in electroanalytical and optical applications.

Acknowledgments

With the contribution of Fondazione Cariplo, grant no. 2011-1851.

References

- [1] T. Benincori, E. Brenna, F. Sannicolò, L. Trimarco, P. Antognazza, E. Cesarotti, (Diphenylphosphino)-biheteroaryls: the first example of a new class of chiral atropisomeric

- chelating diphosphine ligands for transition metal catalysed stereoselective reactions, *J. Chem. Soc., Chem. Commun.* 6 (1995) 685.
- [2] T. Benincori, E. Brenna, F. Sannicolò, L. Trimarco, P. Antognazza, E. Cesarotti, G. Zotti, Chiral atropisomeric five-membered biheteroaromatic diphosphines: New ligands of the bibenzimidazole and biindole series, *J. Organomet. Chem.* 529 (1997) 445.
- [3] T. Benincori, E. Cesarotti, O. Piccolo, F. Sannicolò, 2,2',5,5'-Tetramethyl-4,4'-bis(diphenylphosphino)-3,3'-bithiophene: A new, very efficient, easily accessible, chiral biheteroaromatic ligand for homogeneous stereoselective catalysis, *J. Org. Chem.* 65 (2000) 2043.
- [4] T. Benincori, O. Piccolo, S. Rizzo, F. Sannicolò, 3,3'-Bis-(diphenylphosphino)-1,1'-disubstituted-2,2'-biindoles: Easily accessible, electron-rich, chiral diphosphine ligands for homogeneous enantioselective hydrogenation of oxoesters, *J. Org. Chem.* 65 (2000) 8340.
- [5] J. Wu, C. C. Pai, W. H. Kwok, R. W. Guo, T. T. L. Au-Yeung, C. H. Yeung., A. S. C. Chan, Studies on the rhodium- and ruthenium-catalyzed asymmetric hydrogenation of α -dehydroamino acids using a family of chiral dipyridylphosphine ligand (P-Phos), *Tetrahedron: Asymmetry* 14 (2003) 987.
- [6] L. Vaghi, T. Benincori, R. Cirilli, E. Alberico, P. R. Mussini, M. Pierini, T. Pilati, S. Rizzo, F. Sannicolò, Ph-tetraMe-Bithienine, the first member of the class of chiral heterophosphepines: synthesis, electronic and steric properties, metal complexes and catalytic activity, *Eur. J. Org. Chem.* 36 (2013) 8174.
- [7] F. Sannicolò, S. Arnaboldi, T. Benincori, V. Bonometti, R. Cirilli, L. Dunsch, W. Kutner, G. Longhi, P. R. Mussini, M. Panigati, M. Pierini, S. Rizzo, Potential-driven chirality manifestations and impressive enantioselectivity by inherently chiral electroactive organic films, *Angew. Chem. Int. Ed.* 53 (2014) 2623.

- [8] F. Sannicolò, P. R. Mussini, T. Benincori, R. Cirilli, S. Abbate, S. Arnaboldi, S. Casolo, E. Castiglioni, G. Longhi, R. Martinazzo, M. Panigati, M. Pappini, E. Quartapelle Procopio, S. Rizzo, Inherently chiral macrocyclic oligothiophenes: easily accessible electrosensitive cavities with outstanding enantioselection performances, *Chem. Eur. J.* 20 (2014) 15298.
- [9] G. Longhi, S. Abbate, G. Mazzeo, E. Castiglioni, P. Mussini, T. Benincori, R. Martinazzo, F. Sannicolò, Structural and optical properties of inherently chiral polythiophenes: A combined CD-electrochemistry, circularly polarized luminescence, and TD-DFT investigation, *J. Phys. Chem. C*, 118 (2014) 16019.
- [10] F. M. E. Sannicolò, P. R. Mussini, S. Arnaboldi, E. Quartapelle Procopio, M. Panigati, R. Martinazzo, E. Selli, G. L. Chiarello, T. Benincori, G. Longhi, S. Rizzo, R. Cirilli, A. Penoni, Oligoareni e oligoeteroareni macrociclici elettroattivi ad assi stereogenici, Patent Application MI-2014-A-000948 (23/5/2014).
- [11] S. Arnaboldi, T. Benincori, R. Cirilli, W. Kutner, M. Magni, P. R. Mussini, K. Noworyta, F. Sannicolò, Inherently chiral electrodes: the tool for chiral voltammetry, *Chem. Sci.* 6 (2015) 1706.
- [12] Serena Arnaboldi, *PhD Thesis*, Chiral Electrochemistry in Ionic Liquids, Università degli Studi di Milano, 2014.
- [13] S. Rizzo, S. Menta, C. Faggi, M. Pierini, R. Cirilli, Influence of the nature of alkyl substituents on the high-performance liquid chromatography enantioseparation and retention of new atropisomeric 1,1'-bibenzimidazole derivatives on amylose tris(3,5-dimethylphenylcarbamate) chiral stationary phase, *J. Chromatogr. A* 1363 (2014) 128.
- [14] Bruker, SMART, SAINT and SADABS; Bruker AXS Inc., Madison, Wisconsin, USA, 1997.
- [15] G. M. Sheldrick, A short history of SHELX, *Acta Cryst. A* 64 (2008) 112.

- [16] D. Obermayer, M Damm, C. O. Kappe, Simulating microwave chemistry in a resistance-heated autoclave made of semiconducting silicon carbide ceramic, *Chem. Eur. J.* 19 (2013) 15827.
- [17] I. I. Popov, Investigations of unsaturated azoles. 13. Synthesis and some reactions of 1-alkylbenzimidazoles, *Chem. Heterocycl. Compd.* 32 (1996) 672.
- [18] C. Mukhopadhyay, S. Ghosh, R.J Butcher, An efficient and versatile synthesis of 2,2'-(alkanediyl)-bis-1*H*-benzimidazoles employing aqueous fluoroboric acid as catalyst: density functional theory calculations and fluorescence studies, *Arkivoc* 9 (2010) 75.
- [19] H-L. Wang, R. M. O'Malley, J. E. Fernandez, Electrochemical and chemical polymerisation of imidazole and some of its derivatives, *Macromolecules* 27 (1994) 893.
- [20] D. Minehan, K. A. Marx, S. K. Tripathy, Electrooxidation of imidazole to form soluble electroactive polymer, *Polym. Prepr. (American Chemical Society, Division of Polymer Chemistry)*, 31 (1990) 390.
- [21] C. Hansch, A. Leo, R.W. Taft, A Survey of Hammett substituent constants and resonance and field parameters, *Chem. Rev.* 91 (1991) 165.

Scheme 1. The substrates considered in the present investigation.

Scheme 2. The enantiopure substrates employed for the preliminary enantiorecognition test.

Scheme 3. Two-step reduction of the 2,2'-dimethyl-3-alkyl-[1,1'-bibenzo[*d*]imidazol]-3-ium methanesulfonates (**2a-b**).

Figure captions

Figure 1. CD (left side) and ORD (right side) spectra of (–)-(*R*)-**3a** (green) and (+)-(*S*)-**3a** (red) in methanol.

Figure 2. ORTEP diagram of the asymmetric unit of **1a** (thermal ellipsoids set at the 30% probability level). The co-crystallised water molecule was omitted for clarity.

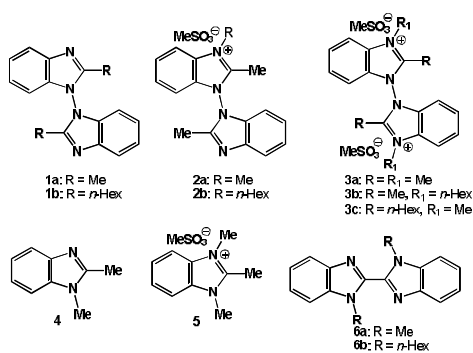
Figure 3. Calculated energy differences between ground and transition states achieved by compound **1a** through rotation around the bond responsible for the N–N ring junction.

Figure 4. Calculated energy profile as a function of the progressive rotation around the bond responsible for the C–C rings-junction in compound **6a**.

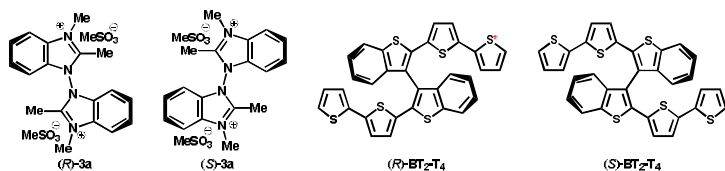
Figure 5. CV patterns of the four model benzimidazole scaffolds **1a**, **1b**, **4**, and **6b** (with detail of scan rate effects), recorded in MeCN + 0.1 M (TEA)BF₄ on GC electrode, at 0.2 V s⁻¹. The thin grey lines represent CVs of the background electrolyte.

Figure 6. CV patterns of the five model benzimidazolium salts **2a**, **2b**, **3a**, **3b**, **3c** and **5**, recorded in MeCN + 0.1 M (TEA)BF₄ on GC electrode, at 0.2 V s⁻¹. The scan rate effect is also reported in four model cases. The thin grey lines represent CVs of the background electrolyte.

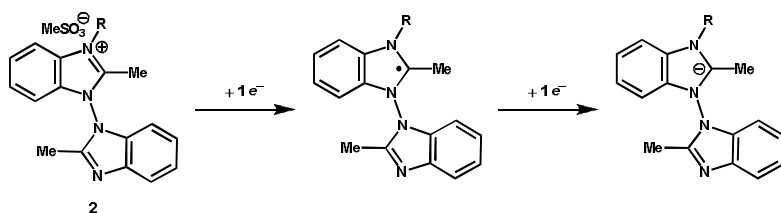
Figure 7. Electrooligomerization tests of 0.0005 M racemic (±)-**BT₂T₄** (above) or enantiopure (*R*)-**BT₂T₄** (below) on GC electrode, in MeCN + 0.1 M (TBA)PF₆, in the absence (red) or in the presence of 2:1 enantiopure (*R*)-**3a** (blue) or (*S*)-**3a** (green).



Scheme 1



Scheme 2



Scheme 3

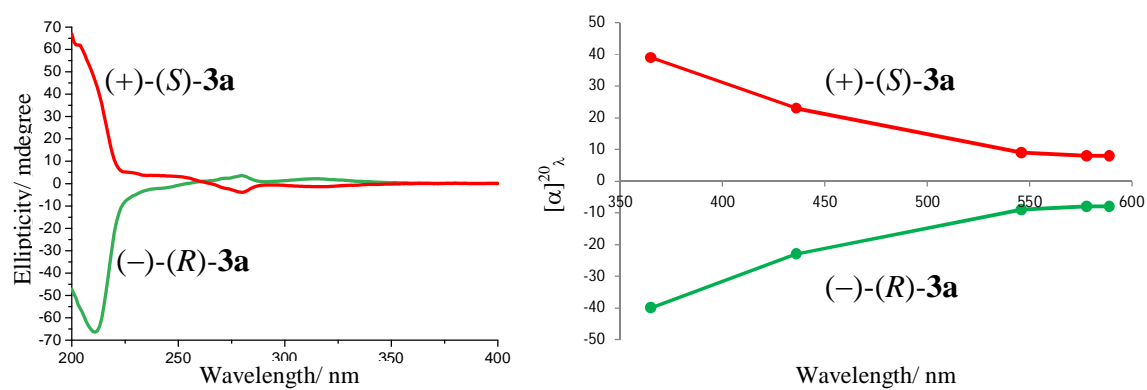


Figure 1

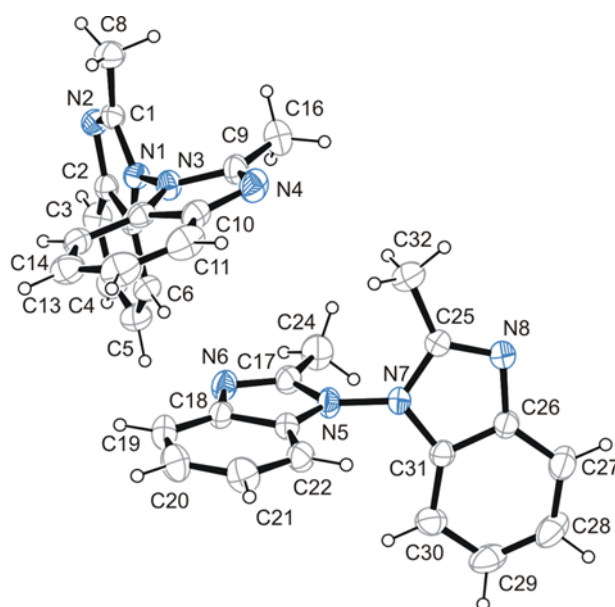


Figure 2

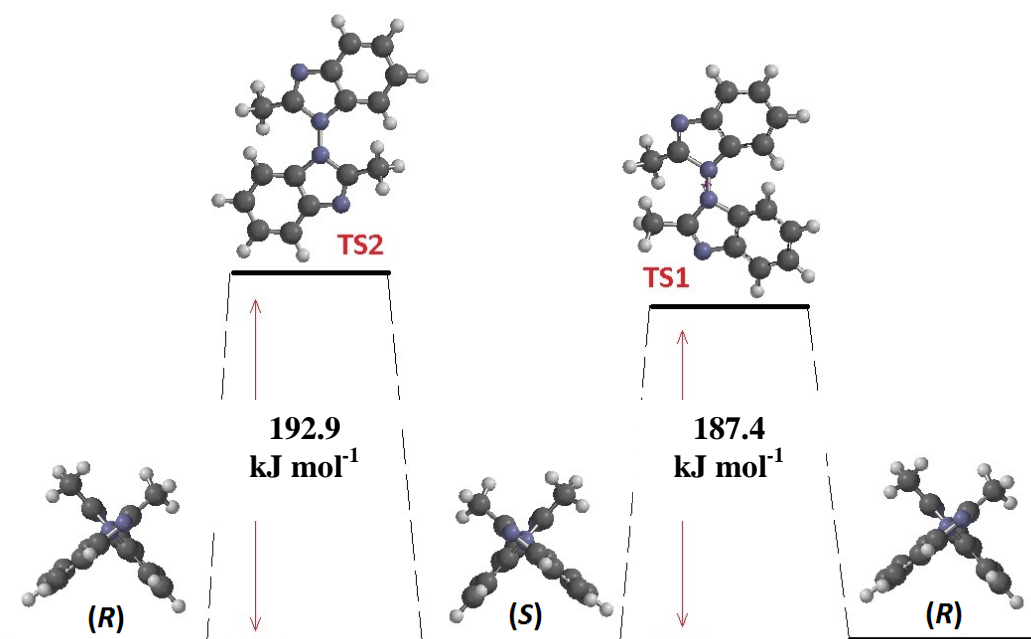


Figure 3

$\Delta E' = 98.0 \text{ kJ mol}^{-1}$ by HF 3-21G method
 $\Delta E' = 92.0 \text{ kJ mol}^{-1}$ by M062X/6-311+G(d,p)//B3LYP/6-31G(d) method

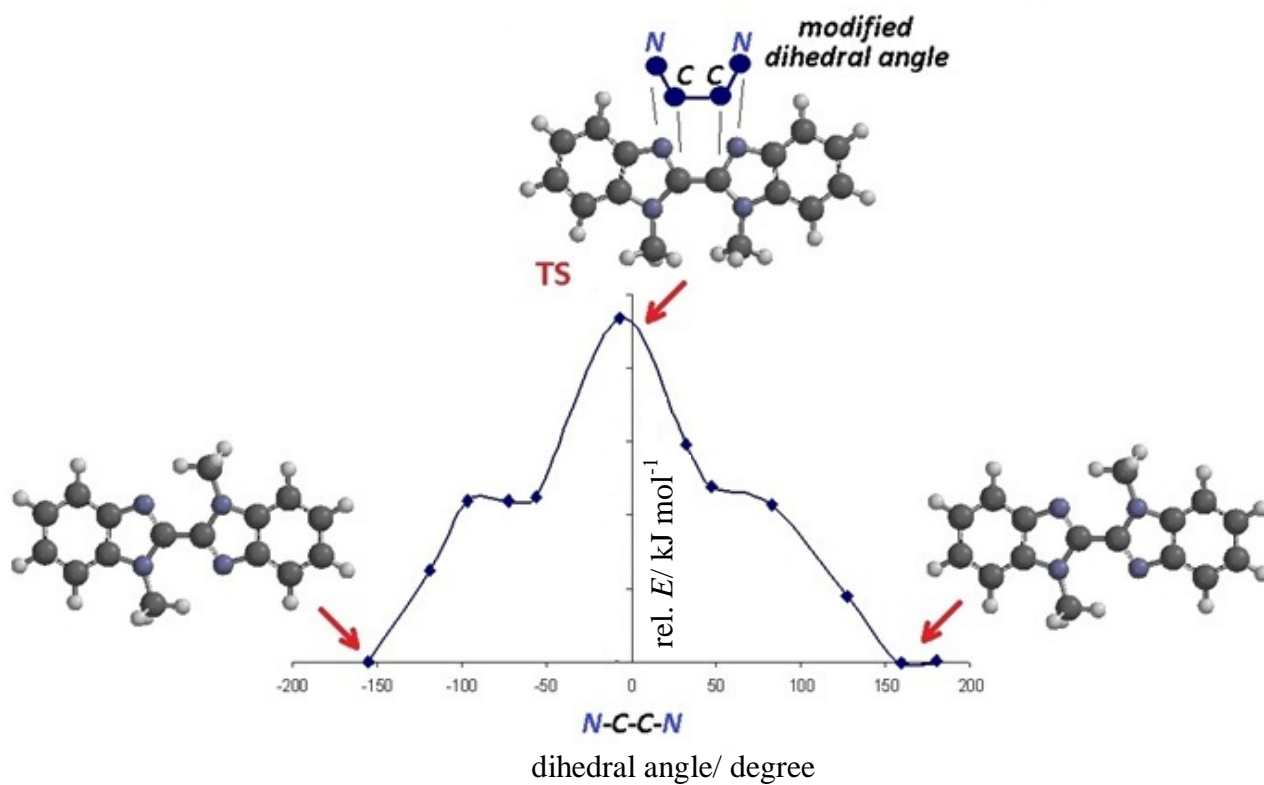


Figure 4

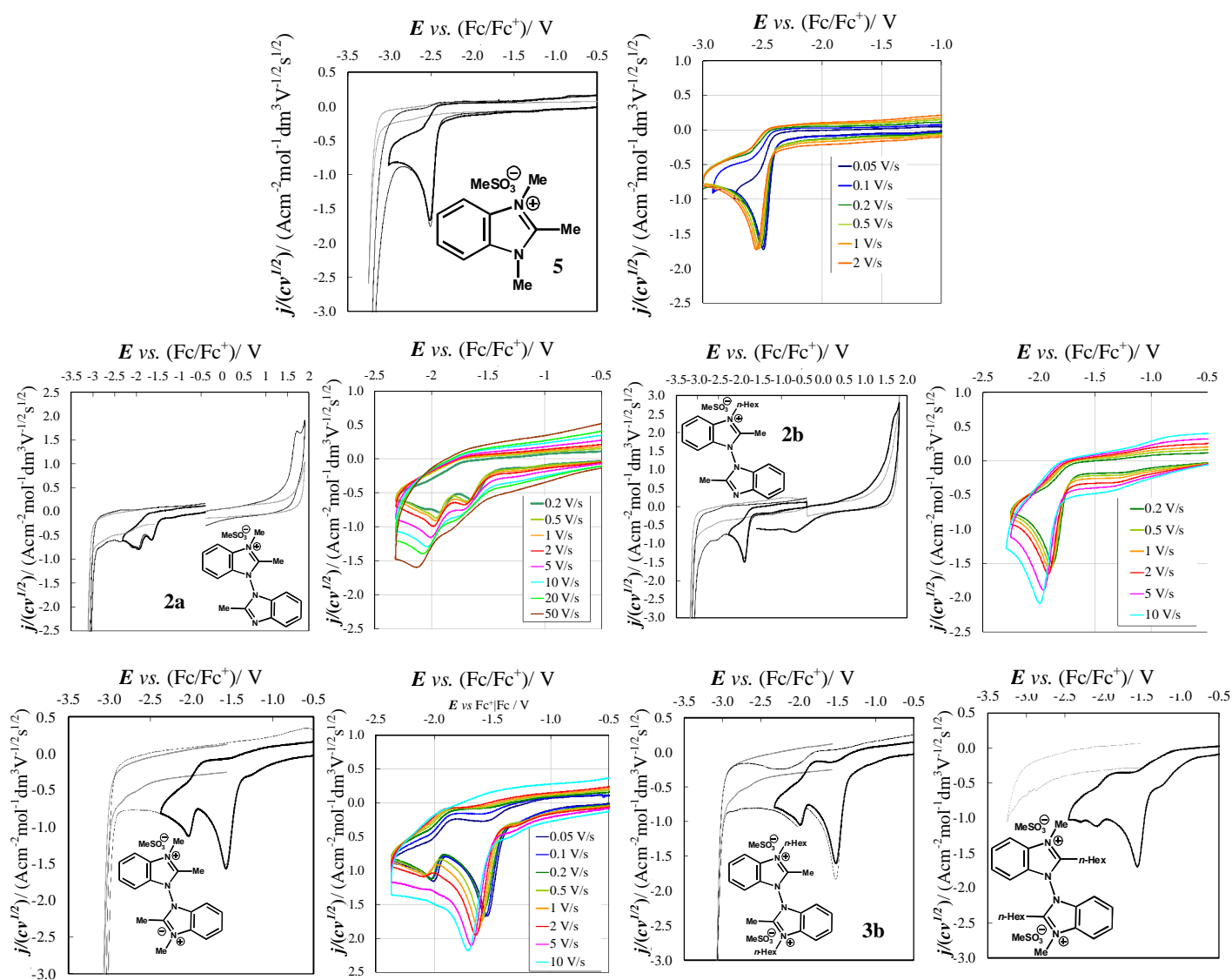


Figure 6

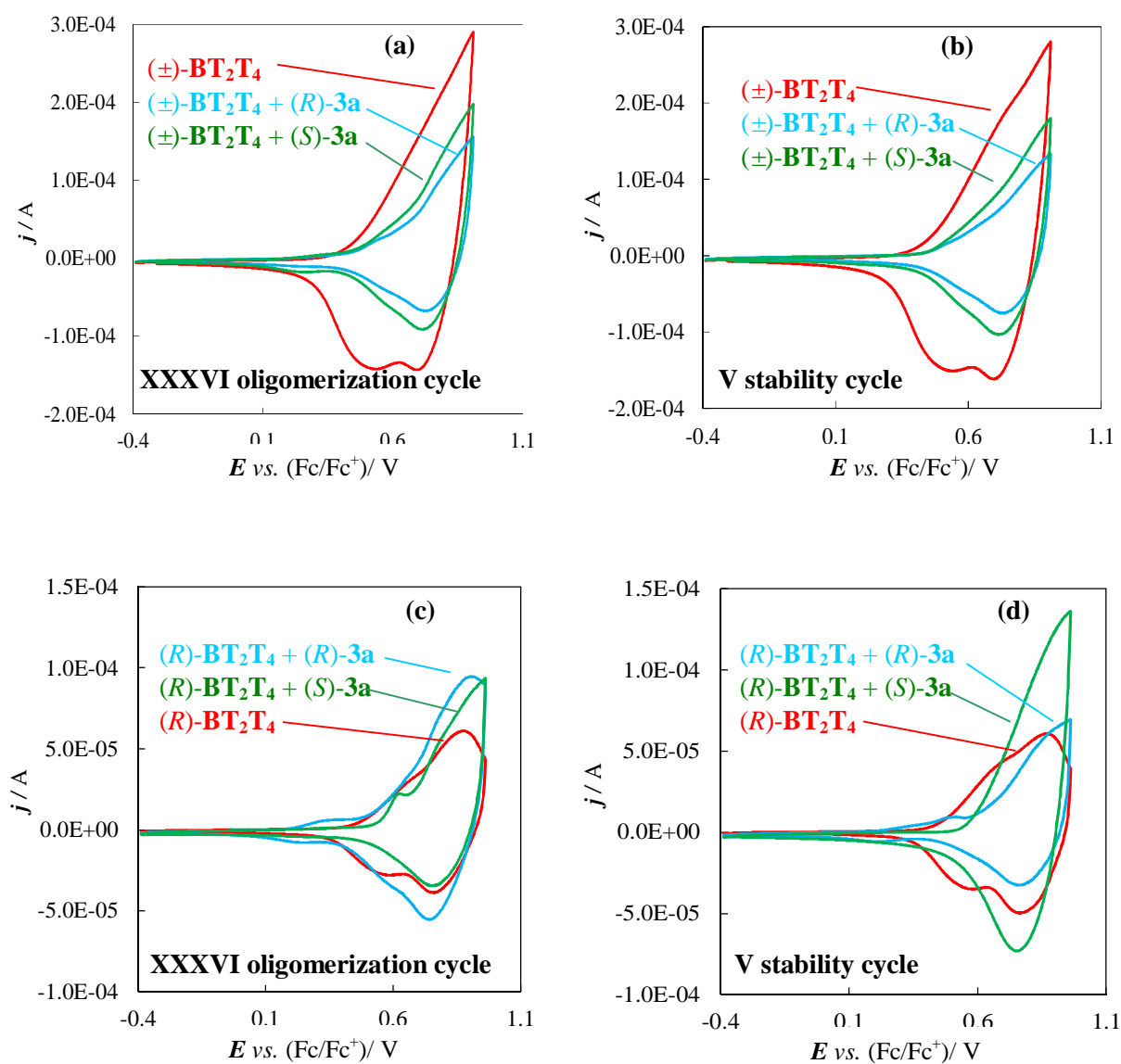
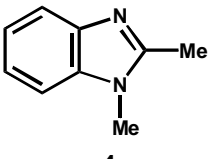
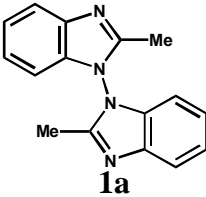
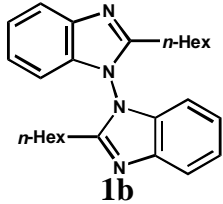
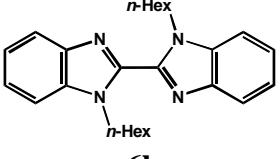


Figure 7

Table 1. Computational methods and energies calculated for (*S*)-**1a** and **6a**, both at the ground state (GS) and transition state (TS)

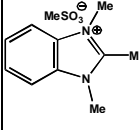
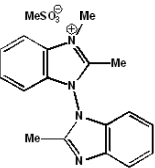
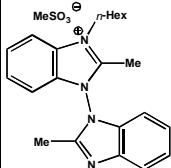
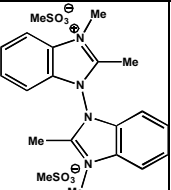
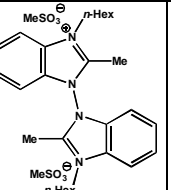
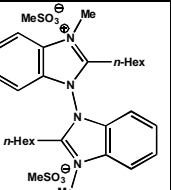
		Computational Method (energies in au)		
		HF/3-21G	B3LYP/6-31G(d)	M062X/6-311+G(d,p)//B3LYP/6-31G(d)
(S)-1a	GS	-	-837.144737	-837.0155265
	TS1	-	-837.073115	-836.9440615
	TS2	-	-837.071460	-836.9420164
6a	GS	-827.214405	-837.178374	-837.0441828
	TS	-827.177061	-837.142059	-837.0090571

Table 2. Key CV parameters for the four model benzimidazole scaffolds **4**, **1a**, **6b**, and **1b**, in MeCN + 0.1 M (TEA)BF₄ on GC electrode.

				
$E_{p,c}$ vs. (Fc/Fc ⁺) / V	< -3.3	-3.02 ^a	-3.08 ^a	-2.65 (I) -2.82 (II)
$j_{p,c} I / (cv^{1/2})$ / (A cm ⁻² mol ⁻¹ dm ³ V ^{-1/2} s ^{1/2})		1.5	1.5	1.5
$E_{p,c} - E_{p,c/2}$ / V		-0.076	-0.074	-0.057
$dE_{p,c} I / d\log v$ / V		-0.054	-0.035	0.004
$E_{p,a}$ vs. (Fc/Fc ⁺) / V	1.13	1.58 ^a	1.52 ^a	1.17 (I) 1.75 (II ^b)
$j_{p,a} / (cv^{1/2})$ / (A cm ⁻² mol ⁻¹ dm ³ V ^{-1/2} s ^{1/2})	1.2			1.5
$E_{p,a} - E_{p,a/2}$ / V	0.068			0.041
$dE_{p,a} / d\log v$ / V	0.040			0.020
$E_{p,a} - E_{p,c}$ / V	>4.4	4.6	4.6	3.82

^aShoulder before background.^bLarge multielectron peak on background.

Table 3. Key CV parameters for of the five model benzimidazolium salts **5**, **2**, **3a**, **3b**, and **3c**, recorded in MeCN + 0.1 M (TEA)BF₄ on GC electrode. E_p and $E_{p/2}$ refer to $v = 0.2 \text{ V s}^{-1}$.

						
$E_{p,c} \text{ vs. (Fc/Fc}^+) / \text{V}$	-2.51	-1.64 (I) -1.92 (II)	-1.88	-1.57 (I) -2.02 (II)	-1.52 (I) -1.98 (II)	-1.56 (I) -2.08 (II)
$j_{p,c1} / (cv^{1/2}) / (\text{A cm}^{-2} \text{ mol}^{-1} \text{ dm}^3 \text{ V}^{-1/2} \text{ s}^{1/2})$	1.4	0.3 (I) ^a 0.4 (II) ^a	1.2	1.2 (I) ^b 0.5 (II) ^b	1.2 (I) § 0.5 (II)§	1.2 (I) ^b 0.65 (II) ^b
$E_{p,cl} - E_{p,cl/2} / \text{V}$	0.055	-0.09 (I) -0.09 (II)	0.077	-0.078 (I) -0.069 (II)	-0.073 (I) -0.067 (II)	-0.078 (I)
$dE_{p,cl} / d\log v / \text{V}$	0.037	-0.065 (I) -0.050 (II)	0.033	-0.059 (I) -0.050 (II)	-0.070 (I) -0.070 (II)	-0.066 (I) -0.066 (II)
$E_{pa} \text{ vs. (Fc/Fc}^+) / \text{V}$	n.d.	1.73	1.69	n.d.	n.d.	n.d.

^aPeak I tends to merge with peak II with increasing scan rate.

^bPeak I increases and peak II decreases with scan rate.